 doi:10.20944/preprints202102.0113.v1

Article

Chromatic Change in Copper Oxide Layers Irradiated with Low Energy Ions

Takuya Kobayashi [1], Fumitaka Nishiyama [2] and Katsumi Takahiro [1,*]

[1] Faculty of Materials Science and Engineering, Kyoto Institute of Technology, Matsugasaki, Sakyo, Kyoto 606-8585, Japan.; m0672011@edu.kit.ac.jp (T.K.)
[2] Research Institute of Nanodevice and Bio Systems, Hiroshima University, Kagamiyama 1-4-1, Higashi-Hiroshima, Hiroshima 739-8527, Japan; fnishi@hiroshima-u.ac.jp
* Correspondence: takahiro@kit.ac.jp

Abstract: The color of a thin copper oxide layer formed on a copper plate was transformed from reddish-brown into blue-purple by irradiation with 5 keV Ar^+ ions to a fluence as low as 1×10^{15} Ar^+ cm^{-2}. In the unirradiated copper oxide layer, the copper valence state of Cu^{2+} as well as Cu^+ and/or Cu^0 was included as indicated by the presence of a shake-up satellite line in a photoemission spectrum. While for the irradiated one, the satellite line decreased in intensity, indicating that irradiation resulted in the reduction from Cu^{2+} to Cu^+ and/or Cu^0. Furthermore, nuclear reaction analysis using a $^{16}O(d, p)^{17}O$ reaction with 0.85 MeV deuterons revealed a significant loss of oxygen (5×10^{15} O atoms cm^{-2}) in the irradiated layer. Thus, the chromatic change observed in the present work originated in the irradiation-induced reduction of a copper oxide.

Keywords: ion beam; copper oxide; chromatic change; photoemission spectrum; beam viewer

1. Introduction

On ion beam experiments including materials analysis and modification with ion beams, a beam monitoring system is installed in the sample chamber to monitor the beam position and uniformity in the beam spot. Most of the beam monitor consists of a fluorescent plate, enabling real time visualization of a beam spot on the plate. A SiO_2 plate, for example, has been used for beam monitoring because of strong emission [1–5] in the visible range when irradiated with MeV-ion beams. A Cr-doped Al_2O_3 (e.g., AF995R, Desmarquest) is also suitable for beam profiling [6,7] for ion beams with energies larger than several hundred keV. The aforementioned materials are insulator and therefore electric charging takes places on the fluorescent plate irradiated with ion beams, resulting in deflection of ion beams in the vicinity of the fluorescent plate if their acceleration voltage is comparable to the charged potential of a few tens kilovolts [8]. This means that the fluorescent point would be different from the real position, and further the fluorescent point would not appear at all in the case of low energy ion beams with < 10 keV. In addition to the fluorescent materials, phosphors such as ZnS based materials [9–11], which have been widely used for screens of a cathode-ray tube, are applicable to beam monitoring. Other candidates of inorganic luminescent materials can be found in the literature [12]. Powders of such materials, mixed with a conducting paste and deposited onto a conducting plate, are candidate for ion beam monitoring materials. However, such powders cost very high, but their lifetimes are very short because radiation damage causes degradation of light-emitting efficiency. It is, therefore, not easy to view a beam spot of a low energy ion beam with energy of several keV on real-time.

On the other hand, non-real time beam monitoring can be conducted by the color change of materials irradiated with ion beams. A polyimide film is, for example, widely used to check both the position and uniformity of an ion beam, because blackening due to graphitization [13–15] occurs when the film is irradiated with ion beams. A polyimide film

Preprints (www.preprints.org) | NOT PEER-REVIEWED | Posted: 3 February 2021 doi:10.20944/preprints202102.0113.v1

is, however, non-conducting and is unapplicable to the beam viewer for low energy ion beams with energies of several keV. The favorable beam viewer for low energy ion beams should be composed of electrically conducting materials. A metallic copper plate, even if a thin upper layer of copper oxide is present, is good conducting material. The color of the copper plate covered with thin oxide is reddish-brown, largely different from polished metallic copper. The present authors made attempt to fabricate a beam viewer in which the appearance of a beam spot turns shiny due to removal of the oxide layer by physical sputtering. In the irradiation apparatus with base pressure of ~2 × 10^{-4} Pa, the shiny beam spot could be clearly recognized after irradiation with 5 keV Ar+ ions to a fluence of 1 × 10^{15} Ar^{+} cm^{-2}. Surprisingly, in the other irradiation equipment with base pressure of ~2 × 10^{-6} Pa, the color of the beam spot turned blue-purple after irradiation under the same conditions above. In the present work, the chromatic change observed in the irradiation equipment with such a high vacuum is examined to fabricate a new type of beam viewer for low energy ion beams.

2. Materials and Methods

Oxygen-free copper plates of 10 × 10 × 1 mm^3 (purity 99.99 %) were supplied from NILACO, Japan. The Cu plate was put on a laboratory hot plate setting to 473 K in ambient air for 2 min to form Cu oxide layer. The maximum temperature measured on the surface with chromel-alumel thermocouple was 440 K, somewhat lower than the setting temperature of 473 K, as recorded in Fig. 1. The color of heat-treated Cu plate was reddish-brown. The samples were irradiated with 5 keV-Ar^{+} ions up to a fluence of 1 × 10^{15} cm^{-2} using a 5 kV-ion gun installed in a vacuum chamber with a base pressure of 2 × 10^{-6} Pa.

X-ray photoelectron spectroscopy (XPS) using Mg Kα radiation ($h\nu$ = 1253.6 eV) was performed with a JEOL 9010 X-ray photoelectron spectrometer (JEOL, Japan) to analyze chemical states of Cu before and after the irradiation. Rutherford backscattering spectrometry (RBS) and nuclear reaction analysis (NRA) using the $^{16}O(d, p)^{17}O$ reaction were conducted for chemical composition analysis with 2 MeV He ions and 0.85 MeV deuterons, respectively, produced from the Van de Graaff accelerator of Hiroshima University. The standard sample for the NRA was a SiO_2 layer formed on a Si wafer (SiO_2/Si), which contains 5.8 × 10^{17} O atoms·cm^{-2} determined by RBS.

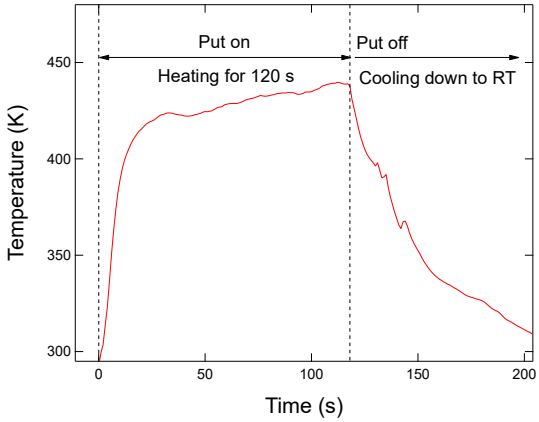

Figure 1. Temperature measured on the sample surface with chromel-alumel thermocouple during oxidation.

3. Results and Discussions

Figure 2 (a) shows a photograph of the sample surface irradiated with Ar^{+} ions to a fluence of 1 × 10^{15} cm^{-2} using a 5 kV ion gun. The color of the sample changed from reddish brown to blue-purple at an irradiation spot. This chromatic change started at the fluence as low as 10^{14} cm^{-2}. On the sample surface irradiated to a fluence of 10^{14} cm^{-2}, the color of

Preprints (www.preprints.org) | NOT PEER-REVIEWED | Posted: 3 February 2021 doi:10.20944/preprints202102.0113.v1

the edge at the beam spot is not clear as can be seen in Fig. 2 (b), indicating that the border between irradiated and unirradiated areas is not so abrupt. Thus, the uniformity of a beam intensity inside the beam spot can be estimated by the uniformity of color.

Figure 2. Photographs of the surface of samples irradiated with 5 keV-Ar+ ions to fluences of 1 ×

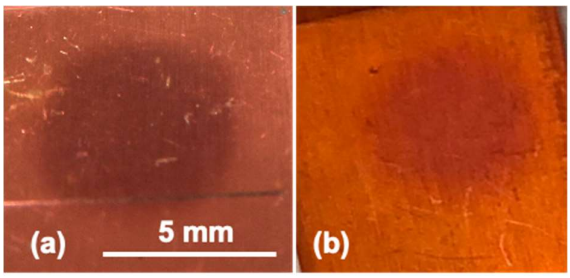

10^{15} cm^{-2} (a) and 1 × 10^{14} cm^{-2} (b).

The mechanism of the observed chromatic change is discussed below, along with RBS, NRA and XPS data. Figure 3 shows the backscattering spectrum of the Cu oxide layer formed on a Cu plate before irradiation. The chemical composition and thickness of the oxide layer was estimated to be $CuO_{0.4}$ and 1.9 × 10^{17} $CuO_{0.4}$ cm^{-2}, respectively, by fitting a simulation spectrum to experimental data, where the program SIMNRA 6.06 [16] was used to obtain the simulation spectrum. The chemical composition $CuO_{0.4}$ indicates that the oxide layer contains the mixture of metallic copper and copper oxides.

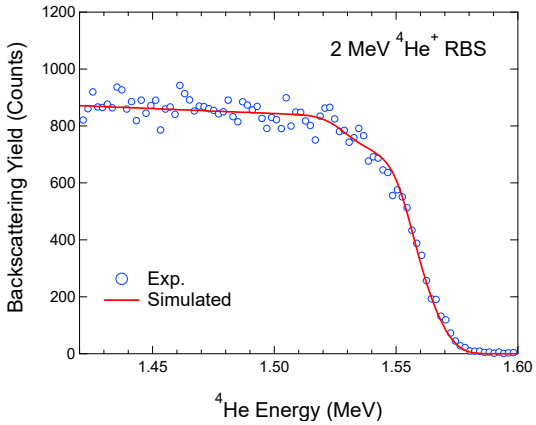

Figure 3. RBS spectrum of the as-prepared sample (blue open circles). A simulated spectrum (red solid line) is also shown.

Figure 4 presents the NRA spectra of the sample with and without irradiation. Peaks located around channel number of 260 correspond to protons emitted by the $^{16}O(d, p)^{17}O$ reaction. The peak intensities are 2.15 × 10^3 and 2.01 × 10^3 counts for the unirradiated and irradiated samples, respectively. The oxygen content in the irradiated sample was determined to be 7.1 × 10^{16} O atoms·cm^{-2} by the SiO_2/Si standard sample, smaller by ~10 % than that in the unirradiated sample (7.6 × 10^{16} O atoms·cm^{-2}). Thus, oxygen atoms were found to be released from the $CuO_{0.4}$ layer by the irradiation with 5 keV-Ar^+ ions to a fluence of 1 × 10^{15} cm^{-2}. The SRIM simulation [17] predicts the sputtering yield of O in $CuO_{0.4}$ to be 4.9 O atoms·ion^{-1}, which means that the sputtered O atoms will be approximately 5 × 10^{15} O atoms·cm^{-2}, corresponding to a difference in the oxygen contents between the unirradiated and irradiated samples. The NRA results and the SRIM calculation suggest that the release of O atoms originates in physical sputtering. In the sputtering process of $CuO_{0.4}$ bombarded with 5 keV-Ar^+ ions, approximately 1.4 × 10^{15} Cu atoms·cm^{-2} as calculated by

Preprints (www.preprints.org) | NOT PEER-REVIEWED | Posted: 3 February 2021 doi:10.20944/preprints202102.0113.v1

the SRIM will be desorbed, leading to the change in chemical composition from $CuO_{0.4}$ to $CuO_{0.38}$ in the layer.

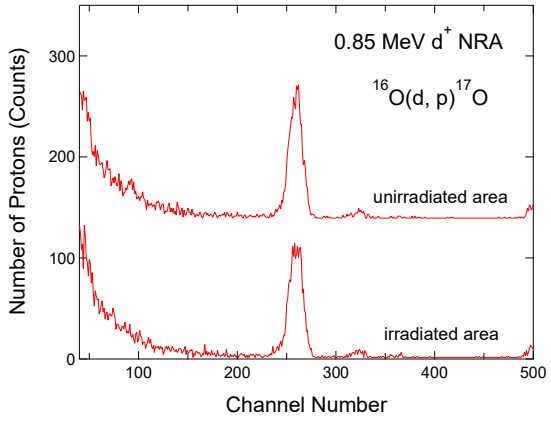

Figure 4. NRA spectra of the unirradiated and irradiated areas in the sample irradiated with 5 keV-Ar+ ions to a fluence of 1×10^{15} cm^{-2}.

Figure 5 shows XPS Cu 2p core level photoemission spectra (PS) of the $CuO_{0.4}$ layer with and without irradiation. As can be seen in Fig. 5, a broad shake-up satellite line due to the charge transfer [18,19] appears in the binding energy (BE) region from 937 to 941 eV of PS for the unirradiated sample and decreases in intensity after irradiation. More quantitatively, the intensity ratio of the satellite to the main line at BE of 932.4 eV was 0.16 and 0.10 for the unirradiated and irradiated samples, respectively. These results indicate that the unirradiated sample includes the copper valence state Cu^{2+} and it is transformed into Cu^{+} and/or Cu^{0} (Cu^{+}/Cu^{0}) by irradiation. Thus the 5 keV-Ar^{+} irradiation reduces Cu^{2+} to Cu^{+}/Cu^{0}. The irradiation-induced reduction observed in the present work can be seen in the change in shape of Cu $2p_{3/2}$ lines before and after irradiation.

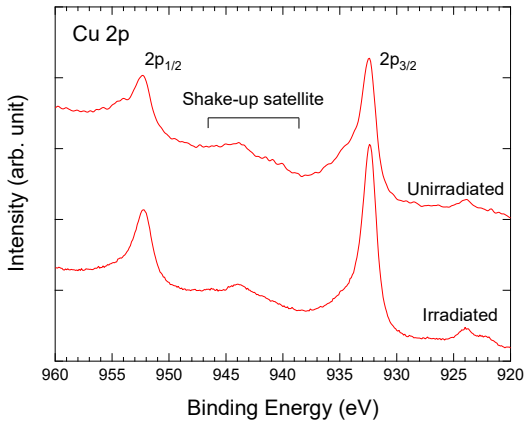

Figure 5. XPS Cu 2p core level photoemission spectra of the unirradiated and irradiated areas in the sample irradiated with 5 keV-Ar+ ions to a fluence of 1×10^{15} cm^{-2}.

Figures 6 (a) and (b) depicts Cu $2p_{3/2}$ lines for the samples before and after irradiation, respectively. Each spectral line consists of three components denoted by I, II and III. The lines, after background subtraction by the Shirly method [20], were decomposed by three Voigt functions using a curve fitting procedure. The component I located at BE of 932.4 eV is assigned to be Cu and/or Cu_2O. The BE of Cu (932.6 eV) [21–23] is very closed to that of Cu_2O (932.5 eV) [24–27], therefore the component I cannot be further decomposed by a curve fitting. The components II and III located at BE of 933.6 eV and 934.8 correspond to

Preprints (www.preprints.org) | NOT PEER-REVIEWED | Posted: 3 February 2021 doi:10.20944/preprints202102.0113.v1

CuO [27–30] and $Cu(OH)_2$ [27,31], respectively. The fractions of each component obtained by the curve fitting are summarized in Table 1 for the samples with and without irradiation. The fractions corresponding to copper valence state Cu^{2+} (CuO and $Cu(OH)_2$) decrease, while the fraction of Cu^+/Cu^0 (Cu_2O/Cu) increases by irradiation, indicating that the Ar^+ irradiation reduces Cu^{2+} to Cu^+/Cu^0. This is consistent with the result deduced from the decrease in intensity of shake-up satellite line as described above.

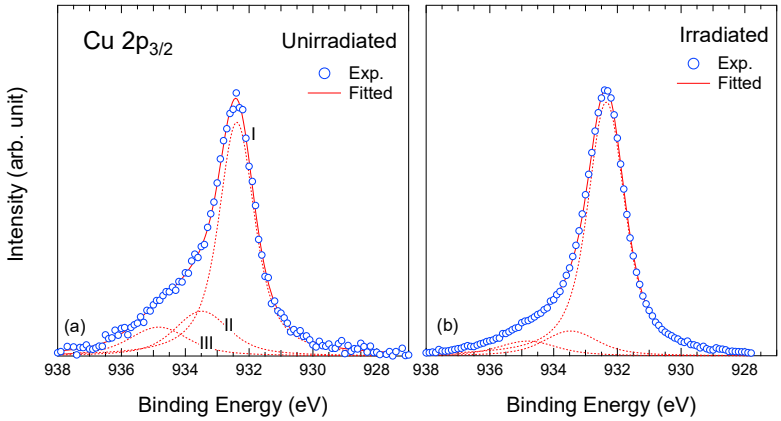

Figure 6. Detailed XPS Cu $2p_{3/2}$ core level photoemission spectra of the unirradiated (a) and irradiated (b) areas in the sample irradiated with 5 keV-Ar+ ions to a fluence of 1×10^{15} cm^{-2}. Each spectrum was decomposed into three components denoted by I, II and III.

The concentration ratio of Cu_2O to Cu can be indirectly determined by the atomic ratio O/Cu of analyzing layer using the fractions of three components. Of course, the O/Cu can be calculated by the intensity ratio of O 1s to Cu 2p PS lines. However, it is impossible to accurately determine the atomic ratio O/Cu because of the presence of adventitious carbon contamination that includes oxygen atoms in the outermost layer. Therefore, the atomic ratio O/Cu in the analyzing layer is assumed to be 0.4 that is determined by RBS, resulting in the concentration ratio Cu_2O/Cu of 8.2/65.7 for the sample without irradiation. These values are presented with parenthesis in Table 1. For the sample with irradiation, the atomic ratio O/Cu in the analyzing layer is definitely different from that in the oxide layer, and thus, the composition $CuO_{0.38}$ determined by the combination of RBS and NRA cannot be used to calculate the fraction of Cu_2O/Cu. Therefore, the fraction of metallic copper is assumed to be unchanged after irradiation. In fact, Panzner et al. [32] demonstrated that the oxide CuO was reduced to Cu_2O, while the oxide Cu_2O was much more stable and no more reduction to Cu occurred under sputtering with 3–5 keV Ar^+ to a low fluence. Then the concentration ratio Cu_2O/Cu is calculated to be 28.4/65.7 for the sample with irradiation. These values are also presented inside parenthesis in Table 1.

Table 1. Compositions of Cu, Cu_2O, CuO and $Cu(OH)_2$ determined by Cu $2p_{3/2}$ PS lines for the unirradiated and irradiated samples.

Samples	Compositions (%)			
	Cu	Cu_2O	CuO	$Cu(OH)_2$
Unirradiated	73.8 (65.7)[1]	(8.1)[1]	16.5	9.7
Irradiated	94.1 (65.7)[1]	(28.4)[1]	5.5	0.4

[1] These values were obtained by the assumption that the composition of the analyzing layer was $CuO_{0.4}$ before irradiation and the fraction of Cu was unchanged after irradiation.

As described above, XPS analysis reveals that the 5 keV-Ar^+ irradiation reduces Cu^{2+} to Cu^+/Cu^0 in the cuprate. This result is consistent with the previous studies that CuO thin films were transformed into Cu_2O by ion irradiation [32,33]. Next, the relationship between the reduction and the chromatic change is discussed.

It is well known that the color of cuprous oxide (Cu_2O) powder is red. In addition, Cu_2O in the form of both thin film [34,35] and nanoparticle [36,36] would be reddish considering their optical absorption spectra. On the other hand, the color of the irradiated layer was found to be blue-purple, different from the color of pure Cu_2O. Fredj and Burleigh [38] showed that the color of a copper oxide layer in which Cu_2O is primarily included varied from bare copper color to green depending on its thickness. The color of the oxide with thickness of ~20 nm was found to be violet blue, similar to the color observed on the irradiated sample in this work. It is, therefore, concluded that the chromatic change observed originates in the presence of a very thin oxide layer that mainly consists of Cu_2O produced by the irradiation-induced reduction from CuO and $Cu(OH)_2$.

As mentioned in Introduction, the beam spot in the sample irradiated with 5 keV-Ar^+ ions using the other machine turned bare copper color due to the removal of an oxide layer by sputtering, different from the present work. The reason for this difference is unknown but may result from the initial composition of the oxide layer. Further studies are needed to clarify the mechanism underlying the irradiation-induced chromatic change in copper oxide layers and to create a new type of beam viewer for low energy ion beams. Such investigations are now in progress using copper oxides with various compositions.

4. Conclusions

The color of a thin copper oxide layer formed on a copper plate turned from reddish-brown to blue-purple by irradiation with 5 keV Ar+ ions to a fluence of 1×10^{15} Ar^+ cm^{-2}. Nuclear reaction analysis revealed that a significant amount of oxygen (5×10^{15} O atoms·cm^{-2}) was released from the irradiated layer. The reduction of cupric oxide (CuO) to cuprous oxide (Cu_2O) occurred in the layer after the irradiation as confirmed by the decrease in intensity of a shake-up satellite line as well as the change in the shape of a Cu $2p_{3/2}$ line in photoemission spectra. The reduction leads to the compositional change in the mixture of $Cu/Cu_2O/CuO$, which results in the chromatic change.

Author Contributions: Conceptualization, K.T. and T.K.; methodology, K.T.; RBS and NRA, F.N.; data curation, T.K. and K.T.; writing—original draft preparation, K.T.; writing—review and editing, K.T. and T.K.; All authors have read and agreed to the published version of the manuscript.

Funding: This research received no external funding.

Conflicts of Interest: The authors declare no conflict of interest.

References

1. Peña-Rodríguez, O.; Crespillo, M.L.; Díaz-Nuñez, P.; Perlado, J.M.; Rivera, A.; Olivares, J. In situ monitoring the optical properties of dielectric materials during ion irradiation. *Opt. Mater. Express* **2016**, *6* 734–742.
2. Rivera, A.; Olivares, J.; Prada, A.; Crespillo, M.L.; Caturla, M.J.; Bringa, E.M.; Perlado, J.M.; Peña-Rodríguez, O. Permanent modifications in silica produced by ion-induced high electronic excitation: experiments and atomistic simulations. *Sci. Rep.* **2017**, *7*, 10641 1–14.
3. Zhou, J.; Li B. Origins of a damage-induced green photoluminescence band in fused silica revealed by time-resolved photoluminescence spectroscopy. *Opt. Mater. Express* **2017**, *7*, 2888–2898.
4. Crespillo, M.L.; Graham, J.T.; Zhang, Y.; Weber W.J. In-situ luminescence monitoring of ion-induced damage evolution in SiO_2 and Al_2O_3. *J. Lumin.* **2016**, *172*, 208–218.
5. Bandourko, V.; Umeda, N.; Plaksin, O.; Kishimoto N. Heavy-ion-induced luminescence of amorphous SiO_2 during nanoparticle formation. *Nucl. Instrum. Meth.* B **2005**, *230*, 471–475.
6. Forck, P.; Andre, C.; Becker, F.; Haseitl, R.; Reiter, A.; Walasek-Höhne, B.; Krishnakumar, R.; Ensinger, W. Scintillation screen investigations for high energy heavy ion beams at GSI. Proceedings of DIPAC2011, Hamburg, Germany, 170–172.
7. Johnson, C.D. The development and use of alumina ceramic fluorescent. European Laboratory for Particle Physics, CERN/PS/90-12(AR), Geneva, Switzerland, 1990.

8. Takahiro, K., Terai A.; Kawatsura, K.; Naramoto, H.; Yamam, S.; Tsuchiya, B.; Nagata, S.; and Nishiyama, F. Rutherford backscattering spectrometry of electrically charged targets: Elegant technique for measuring charge-state distribution of backscattered Ions. *Jpn. J. Appl. Phys.* **2006**, *45*, 1823–1825.
9. Parajuli, R. K. Kada, W.; Kawabata, S.; Matsubara, Y.; Sakai, M.; Miura, K.; Satoh, T.; Koka, M.; Yamada, N.; Kamiya, T.; Hanaizumi, O. O. Ion-Beam-Induced Luminescence Analysis of β-SiAlON:Eu Scintillator under Focused Microbeam Irradiation. *Sensor Mat.* **2016**, *28*, 837–844.
10. Warren, A.J.; Thomas, C.B.; Reehal, H.S.; Stevens P.R.C. A study of the luminescent and electrical characteristics of films of ZnS doped with Mn. *J. Lumin.* **1983**, *28*, 147–162.
11. Calusi, S.; Colombo, E.; Giuntini, L.; Giudice, A. L.; Manfredotti, C.; Massi, M.; Pratesi, G.; Vittone, E. The ionoluminescence apparatus at the LABEC external microbeam facility. *Nucl. Instrum. Meth.* B **2008**, *266*, 2306–2310.
12. Feldmann, C.; Jüstel, T.; Ronda, C.R.; Schmidt, P.J. Inorganic Luminescent Materials: 100 Years of Research and Application. *Adv. Funct. Mater.* **2003**, *13*, 511–516.
13. Jacob, K.; Zelina, I.; Leonid, K.; Dennison, Jr.; Brian, W.; Grigorievsky; Carl, B. Long-term stability of ion-beam treated space polymers in geo-simulated environment. Proceeding of the 14th ISMSE $ 12th ICPMSE, Biarritz, France, 1–5 Oct. 2018.
14. Plis, E.A.; Engelhart, D.P.; Cooper, R.; Johnston, W. R.; Ferguson, D.; Hoffmann, R. Review of Radiation-Induced Effects in Polyimide. *Appl. Sci.* **2019**, *9*, 1999 1–23.
15. Matienzo, L.J.; Emmi, F.; Van Hart, D.C.; Gall, T. P. Interactions of high-energy ion beams with polyimide films. *J. Vac. Sci. Technol.* A **1989**, *7*, 1784–1789.
16. Computer simulation of RBS, ERDA, NRA, MEIS and PIGE by Matej Mayer, available online: https://home.mpcdf.mpg.de/~mam/Version6.html.
17. Ziegler, J.F.; Ziegler, M.D.; Biersack, J.P. SRIM – The stopping and range of ions in matter (2010). *Nucl. Instrum. Meth.* B **2010**, *268*, 1818–1823.
18. Kawai, J.; Tsuboyama, S.; Ishizu, K.; Miyamura, K.; Saburi, M. Covalency of copper complex determined by Cu 2p X-ray photoelectron spectrometry. *Anal. Sci.* **1991**, *7 Supple*, 337–340.
19. Pawar, S.M.; Kim, J.; Inamdar, A.I.; Woo, H.; Jo, Y.; Pawar, B.S.; Cho, S.; Kim, H.; Im, H. Multi-functional reactively-sputtered copper oxide electrodes for supercapacitor and electro-catalyst in direct methanol fuel cell applications. *Sci. Rep.* **2016**, *6*, 21310 1–9.
20. Végh J. The Shirley background revised. *J. Electron Spectrosc. Relat. Phenom.* **2006**, *151*, 159–164.
21. Anderson, C.R.; Lee, R.N. Comparison of APS and FRESCA core level binding energy measurements. *J. Vac. Sci. Technol.* **1982**, *20*, 617–621.
22. Seah, M.P.; Gilmore, I. S.; Beamson, G. XPS: binding energy calibration of electron spectrometers 5—re-evaluation of the reference energies. *Surf. Interface Anal.* **1998**, 26, 642–649.
23. Bird, R.J.; Swift, P. Energy calibration in electron spectroscopy and the re-determination of some reference electron binding energies. *J. Electron Spectrosc. Relat. Phenom.* **1980**, *21*, 227–240.
24. McIntyre, N.S.; Cook, M.G. X-ray photoelectron studies on some oxides and hydroxides of cobalt, nickel, and copper. *Anal. Chem.* **1975**, *47*, 2208–2213.
25. Schön, G. ESCA studies of Cu, Cu2O and CuO. *Surf. Sci.* **1973**, *35*, 96–108.
26. Losev, A.; Rostov, K.; Tyuliev, G. Electron beam induced reduction of CuO in the presence of a surface carbonaceous layer: an XPS/HREELS study. *Surf. Sci.* **1989**, *213*, 564–579.
27. Deroubaix, G.; Marcus, P. X-ray photoelectron spectroscopy analysis of copper and zinc oxides and sulphides. *Surf. Interface Anal.* **1992**, *18*, 39–46.
28. Haber, J.; Machej, T.; Ungier, L.; Ziółkowski, J. ESCA studies of copper oxides and copper molybdates. *J. Solid State Chem.* **1978**, *25*, 207–218.
29. Gaarenstroom, S.M.; Winograd, N. ESCA spectra of cadmium and silver oxides. *J. Chem. Phys.* **1977**, *67*, 3500–3506.
30. Tobin, J.P.; Hirschwald, W.; Cunningham, J. XPS and XAES studies of transient enhancement of Cu[1] at CuO surfaces during vacuum outgassing. *Appl. Surf. Sci.* **1983**, *16*, 441–452.
31. Biesinger M.C. Advanced analysis of copper X-ray photoelectron spectra. *Surf. Interface Anal.* **2017**, *49*, 1325–1334.
32. Panzner, G.; Egert, B.; Schmidt, H.P. The stability of CuO and Cu_2O surfaces during argon sputtering studied by XPS and AES. *Surf. Sci.* **1985**, *151*, 400–408.
33. Dementyeva, M.M.; Prikhodko, K.E.; Gurovich, B.A.; Bukina, Z.V.; Komarov, D.A.; Kutuzov, L.V. Phase transitions in copper oxide thin films under proton irradiation. *IOP Sonf. Ser.: Mater. Sci. Tecnol.* **2017**, *256*, 012020 1–5.
34. Pan, J.; Yang, C.; Gao Y. Investigations of Cuprous Oxide and Cupric Oxide Thin Films by Controlling the Deposition Atmosphere in the Reactive Sputtering Method. *Sensor Mat.* **2016**, *28*, 817–824.
35. Gevorkyan, V.A.; Reymers, A.E.; Nersesyan, M.N.; Arzakantsyan, A.M. Characterization of Cu_2O thin films prepared by evaporation of CuO powder. *J. Phys.: Conf. Ser.* **2012**, *350*, 012027 1–6.
36. Goua, L.; Murphy, C.J. Controlling the size of Cu_2O nanocubes from 200 to 25 nm. *J. Mater. Chem.* **2004**, *14*, 735–738.
37. Butte, S.M.; Waghuley, S.A. Optical properties of Cu_2O and CuO. *AIP Conf. Proc.* **2020**, 2220, 020093 1–5.
38. Fredj, N.; Burleigh, T.D. Transpassive Dissolution of Copper and Rapid Formation of Brilliant Colored Copper Oxide Films. *J. Electrochem. Soc.* **2011**, *158*, C104–C110.